ELSEVIER

Journal of Atmospheric and Solar-Terrestrial Physics 68 (2006) 1502–1519

Journal of ATMOSPHERIC AND SOLAR-TERRESTRIAL PHYSICS

www.elsevier.com/locate/jastp

The application of ground-based optical techniques for inferring electron energy deposition and composition change during auroral precipitation events

J.H. Hecht[a,*], D.J. Strickland[b], M.G. Conde[c]

[a]*Space Science Applications Laboratory, The Aerospace Corporation, Los Angeles, CA 90009, USA*
[b]*Computational Physics Inc., Springfield, VA 22151, USA*
[c]*Physics Department, La Trobe University, Victoria 3086, Australia*

Available online 16 June 2006

Abstract

Passive ground-based optical techniques have been used for over 15 years to study the effects of auroral energy deposition on the composition of the lower thermosphere. These techniques typically involve measuring bright auroral emissions that depend on the number density of atomic oxygen [O] and molecular nitrogen [N_2] as well as the energy flux and energy spectrum of the precipitating auroral particles. Here we review the application of these techniques to the composition problem. In particular, we present data obtained from photometric observations in Alaska and Greenland in the 1980s and 1990s. While some of these results are available in the existing literature, some are new and have not been presented before. Recent results from Alaska obtained in support of the TIMED satellite are also presented. The data as a whole suggest that the ratio of column integrated [O] to [N_2] above a given site decreases as the total energy fluence from both auroral particle and Joule heating increases. However, the dependence is complicated by effects such as the prior history of disturbance and by horizontal transport due to neutral winds; it is not yet determined if composition responds linearly to energy fluence even in an average sense.

Keywords: Atmospheric composition; Aurora; Thermosphere; Geomagnetic storms

1. Introduction

One poorly addressed problem in aeronomy is how to quantify the effects of auroral energy input upon local thermospheric composition, especially in the region between 100 and 200 km altitude. Existing satellite mass spectrometer measurements do give a global statistical picture of these effects above approximately 150 km. These data form the basis for the empirical Mass Spectrometer and Incoherent Scatter (MSIS) models (e.g. Hedin, 1983). Using boundary conditions, these models extend predictions of composition down below 100 km. However, by their very nature the MSIS model predictions are only representative of large spatial and long temporal scales. For example, the shortest time scale in MSIS is dictated by 3 h a_p values used to derive the model. The use of a_p is itself a global parameter, which can obscure the local input of auroral energy that can occur during a 1–2 h auroral substorm.

*Corresponding author. Fax.: +1 310 5638232.
E-mail address: james.hecht@aero.org (J.H. Hecht).

1364-6826/$ - see front matter © 2006 Elsevier Ltd. All rights reserved.
doi:10.1016/j.jastp.2005.06.022

As Christensen et al. (1997) have pointed out, the qualitative effects of auroral energy input have been known for a long time. Energy is deposited into the atmosphere due to dissipation of electric currents, known as Joule heating, and due to the dissipation of kinetic energy from precipitating particles. These energy losses cause circulation cells to form, vertical winds to increase in the vicinity of the heating, and subsequent uplifting of air parcels containing relatively little atomic oxygen. At a given altitude above the heating this results in a reduction of the ratio of light molecular weight species to heavy molecular weight species (e.g., Hays et al., 1973; Mayr and Volland, 1973; Fuller-Rowell, 1985). Certainly, for large geomagnetic storms and at altitudes above 150 km, such effects are found in the predictions of the MSIS models. Similar effects should also be seen on a more local scale during and after auroral substorms. Deposition of auroral energy should drive vertical circulation resulting in changes in atmospheric composition.

While disturbed composition first occurs above the heated regions, strong winds in the auroral zone can transport it both zonally and equatorward to midlatitudes. Under the right conditions atomic oxygen depleted patches can span tens of degrees in both latitude and longitude. Downwelling at lower latitudes, however, can also produce the opposite effect (Burns et al., 1995). Examples of papers addressing these problems through the use of global circulation modeling efforts are Burns et al. (1991, 1995) and Fuller-Rowell et al. (1994, 1996). Global satellite measurements have confirmed that particle and Joule heating during geomagnetic substorms can produce significant upwelling of air from the lower thermosphere, leading to depletions in the column density of atomic oxygen over large geographical regions outside auroral regions. These have been seen by the DE-1 FUV imager (e.g., Craven et al. (1994), Nicholas et al. (1997), Immel et al. (1997), Strickland et al. (1999), and Drob et al. (1999)).

The recent Thermosphere Ionosphere Mesosphere Energetics and Dynamics (TIMED) satellite mission attempts to measure the basic state of the Mesosphere and Lower Thermosphere (MLT) globally, and especially in the region below 150 km (Christensen et al., 2003). The data obtained by TIMED instruments determine, globally, the circulation pattern in the MLT region as well as composition and electrical conductivities. Thus, TIMED data address the problem of how large inputs of energy into the atmosphere via particle input and Joule heating affect the global MLT atmospheric composition globally. There are two limitations, however, with the TIMED approach. One is the current inability to obtain lower thermospheric composition data in the nightside auroral zone, the region where large auroral energy deposition occurs. This capability does exist with the Global Ultraviolet Imager (GUVI) instrument but is not currently part of the GUVI plan and if it is utilized, that mode will need validation. The second problem, inherent in any low-altitude remote sensing satellite is that the TIMED measurements for a given geographic location are only a brief snapshot of what is often a dynamic situation.

Over the past 15 years a number of techniques have been applied to measure atmospheric composition changes in the lower thermosphere due to auroral precipitation. Some of these involve rocketborne optical measurements (Hecht et al., 1995; Strickland et al., 2000) which are of course impractical for long duration monitoring experiments. Ground-based passive optical techniques offer the possibility of more continuous monitoring of the effects of auroral precipitation on composition change in the lower thermosphere, and at much lower cost.

Strickland et al. (1989) developed a ground-based technique where, by measuring the brightness of three auroral optical emissions, three important aeronomic parameters could be determined. The first of these is the total energy flux, Q, which has units of $\mathrm{mW\,m^{-2}}$. The second, E_0, has units of keV and is the characteristic energy of either a Maxwellian or Gaussian electron energy distribution. The third, f_O, is a dimensionless scaling factor that multiplies the entire atomic oxygen profile of a given model atmosphere and thus, as discussed below, gives a measure of the perturbation of the ratio of the number density of atomic oxygen [O] integrated over the entire column to the number density of molecular nitrogen [N_2] also integrated over the entire column. Since auroral energy deposition altitudes are often in the 100–200 km altitude region, this technique provides a way of monitoring composition change, specifically, [O]/[N_2] in the lower thermosphere (Strickland et al., 1989; Hecht et al., 1989). This paper will review the use of this technique and its past and current usefulness in studying composition change due to auroral precipitation.

2. Experimental technique

2.1. Background

In the initial approach advocated by Strickland et al. (1989) three emission brightnesses were to be monitored in the direction of the magnetic zenith; the permitted N_2^+ (427.8 nm) first negative group (1NG) 0,1 molecular band emission also referred to as the blue emission, the forbidden OI (630.0 nm) atomic oxygen emission line also referred to as the red emission, and the permitted OI (844.6 nm) atomic oxygen emission line also referred to as the 844.6 emission. An alternative to the latter was to measure the spectral lineshape of the permitted OI (777.4 nm) emission. This had to be measured with a Fabry–Perot interferometer with significant integration time (minutes) as opposed to the other three emissions, which could be measured with photometers with integration times of seconds (Hecht et al, 1989). Thus, while reference will be made to the OI (777.4 nm) measurements, this review will concentrate on the strengths and weaknesses of the photometer approach which is a candidate for implementation at future passive optical auroral observatories.

The blue emission originates mainly in the lower thermosphere between 100 and 200 km. Its brightness, measured in a narrow-field centered on the magnetic zenith, can be used to infer the particle energy flux, Q, provided that an estimate is also available of the characteristic energy of the precipitating auroral particles. The red emission is severely quenched below 200 km; it was thus proposed that a ratio of the red to blue emissions could be used as an indicator of E_0 (e.g., Rees and Luckey, 1974). However, the red emission does depend somewhat on [O] (albeit above 200 km) while the blue emission depends on [N_2] (albeit much below 200 km) and thus this ratio is not entirely independent of composition. Like the blue, the 844.6 emission also originates mainly from the lower thermosphere, but depends mostly on [O]. Thus the Strickland et al. (1989) approach was to plot the ratio of red/blue to 844.6/blue (or in its original form the narrow component of the OI (777.4 nm) emission to blue) to obtain not only E_0, but also a measure of the composition parameter f_O. Fig. 1 shows a typical plot of red/blue vs. 844.6/blue with curves for E_0 and f_O indicated. The model is the generic moderate activity atmosphere used for GUVI analysis of data obtained over Poker Flat, Alaska (D. Strickland, private communication, 2004). The Strickland et al. (1989) calculations, which use an electron transport model and full chemistry, also suggest that even though the red emission does depend on [O], it is less sensitive than the 844.6 emission. This technique therefore offers a method for probing atmospheric composition change between 100 and 200 km. Despite the promise, this new method for probing this region of the atmosphere does not enjoy extensive use.

There are three potential problems with this approach. Gattinger et al. (1991) addressed the first of these, namely, atmospheric scattering effects that can be large under certain adverse conditions. They noted that as much light is scattered into as out of the field-of-view where the sky is uniformly covered by aurora (diffuse aurora) but that other geometries were more difficult to analyze. Using a set of well-calibrated data taken at the incoherent radar site located at Sondre Stromfjord, Greenland, they showed that by measuring two molecular nitrogen emissions well separated in wavelength, such as the blue and the N_2 first positive group (1PG) 2,1 band at 871.0 nm (hereafter also referred to as 871.0), several important characteristics of scattering could be accounted for since the ratio of these two emissions should, except during highly energetic aurora, stay constant. Using this blue/871.0 ratio, it became possible to identify: (1) periods of uniform diffuse aurora, where the ratio should be its nominal model value; (2) periods where bright aurora occur over the field of view, where the blue/871.0 ratio should be below its nominal value because more blue than 871.0 emission is scattered out of the field of view; and (3) periods where bright structured aurora are just outside the field of view, where the ratio increases above the nominal value because more blue than 871.0 is scattered into the field of view. When non-nominal blue/871.0 ratios are encountered blue and red are corrected following the model procedure outlined in Hecht et al. (1999). The 844.6 emission is not corrected as it is assumed to scatter similar to 871.0. Thus one can use the blue/871.0 ratio to both identify periods where atmospheric scattering effects are important and, in principle, to correct for them.

Second, OI (844.6 nm) has an additional excitation mechanism, electron impact on O_2. While this is small compared to the electron impact on O excitation, it might distort the results under certain conditions. For this reason much of the early analysis in the Hecht et al. (1989) paper

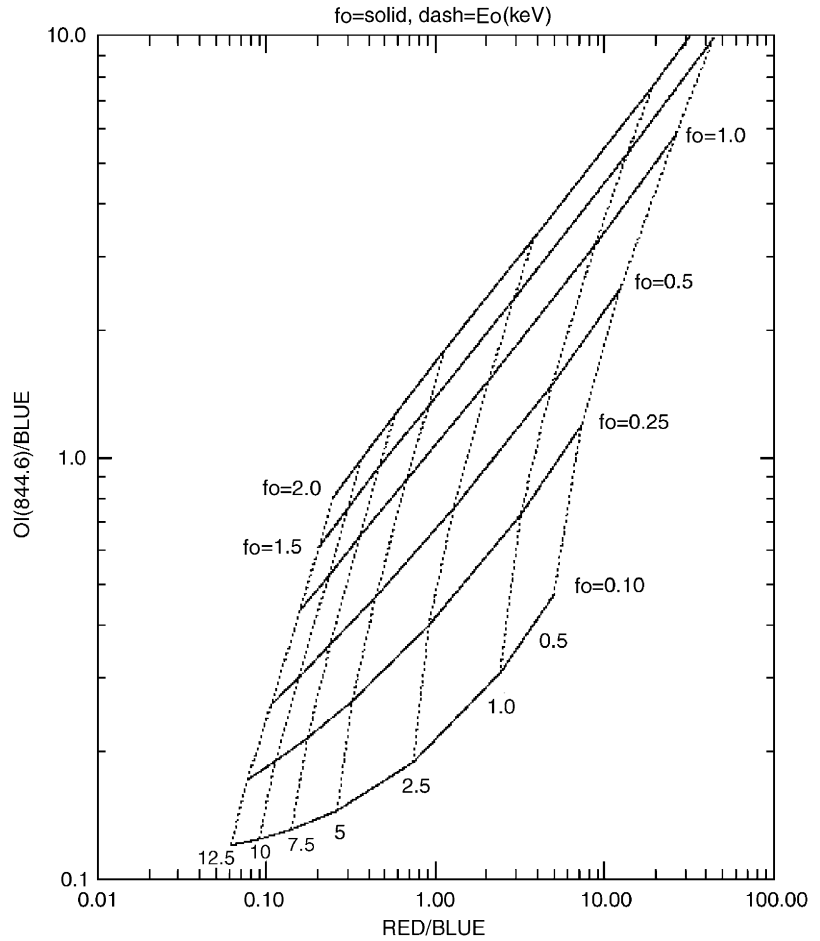

Fig. 1. A plot of the red/blue vs. 844.6/blue ratio as a function of E_0 and f_O for an MSIS-90 atmosphere (A_p of 30, F10.7 of 180 over Poker Flat, Alaska near local midnight). Characteristic energies (E_0), shown at the base of each dotted line, refer to electron precipitation characterized by Gaussian energy distributions with high and low energy tails (Strickland et al., 1993).

concentrated on measurement of the so-called narrow component of the OI (777.4 nm) emission, which is excited by electron impact on oxygen atoms, to form the ratio of OI (777.4 nm) to blue. Unlike OI (844.6 nm), which can be measured with a photometer, the lineshape of OI (777.4 nm) must be measured with a Fabry–Perot interferometer. This is because the atomic oxygen excited component, which may be only a small fraction of the total emission, can only be separated from the molecular oxygen excited component by measuring the lineshape as shown in Hecht et al. (1985). However, data taken during the great magnetic storm of 1986 (Hecht et al., 1991) showed good agreement between results using photometric measurements of OI (844.6 nm) and the Fabry–Perot measurements using OI (777.4 nm). Theoretically, unless the atmosphere is highly depleted in O relative to ambient conditions, about 80–90% of the OI (844.6 nm) emission typically arises from the atomic oxygen excitation. As the percentage decreases, however, because of strong O depletion during very large storms (A_p above 100), the technique may underestimate the depletion due to the excess OI (844.6 nm) emission from dissociative excitation of O_2 unless this process is taken into account. The auroral emission ratio plots such as Fig. 1 do in fact include this dissociative emission component although it is generally small (less than 25% of the total even when E_0 is 10 keV) compared to the O excited component. But it should be noted that the dissociative emission component is tied to the O_2/N_2 density ratio, and that this ratio does exhibit some degree of variation under changing solar and geomagnetic conditions based on the various versions of the MSIS model. In spite of this

complication, it is anticipated that whatever model atmosphere is selected for constructing auroral emission ratio plots, this emission component is adequately accounted for within the overall error budget associated with the derivation of E_0 and f_O. Because of the ease of making photometric OI (844.6 nm) measurements, this is the method of choice for automated continuous measurements.

Third, there was some uncertainty at the time of the 1989 work regarding details of the red line chemistry. While this was addressed in a companion paper by Meier et al. (1989), it was felt that initial measurements of atmospheric composition change should not be burdened by additional uncertainties of excitation mechanisms. Thus, the first application of the technique actually did not use the red/blue ratio but rather obtained E_0 from simultaneous incoherent scatter radar measurements at Sondre Stromfjord (Kangerlussaq), Greenland and then used 844.6 to blue to obtain f_O (e.g. Niciejewski et al., 1989; Hecht et al., 1991). However, in both of these studies, the red/blue data seemed to be in agreement with the Strickland model predictions. More significantly, during the atmospheric response in aurora 1 (ARIA 1) rocket campaign at Poker Flat, Alaska (Anderson et al., 1995) the E_0 derived during a stable diffuse aurora using the red/blue versus 844.6/blue technique agreed with the in situ rocket measurements made by an onboard electron spectrometer (Hecht et al., 1995). The ground-based result for f_O, derived using the ground-based red/blue versus 844.6/blue technique, was about 10% higher than the f_O derived using the in situ rocket measurements for E_0 and 844.6/blue. A more convincing study was done by Hecht et al. (1999) who compared the E_0s derived from ISR data at Kangerlussaq with the E_0s inferred from the four photometer emission techniques (blue, red, 844.6, and 871.0) and found good agreement. More recent comparisons and potential problems will be discussed at the end of this review.

Alternative ground-based techniques exist to the purely photometric technique described above especially for measuring E_0. Any auroral emission will have an average temperature that depends on E_0. This has long been known (e. g. Vallance Jones, 1974) and has been exploited in the literature mainly with respect to the rotational temperature of the blue emission (see e.g., Vallance Jones et al., 1987; Niciejewski et al., 1989; Gattinger et al., 1991). Of particular interest is the work of Sivjee and colleagues (see for example Sivjee and Shen, 1997; Sivjee et al., 1999) who have exploited this method for a number of interesting studies. They use spectrometer measurements which measure a number of N_2, O_2, and atomic species to derive E_0 and f_O. Because modern CCD-based spectrometers can be fast, auroral spectra can be obtained in a few tens of seconds at adequate resolution to measure the bright auroral species needed in the Strickland technique. Thus, this should be considered as an alternative to the photometric technique although the latter may be somewhat cheaper, more robust, and also provide information about scattering due to clouds which is important for automated operation.

Another variation on this is the Scanning Doppler Imaging Fabry–Perot developed at Poker Flat Observatory, Alaska (Conde and Smith, 1998). This instrument measures the line profile of the OI (557.7 nm) green line which allows an inference of E_0 from the measured temperature (M. Conde, private communication, 2004). A great advantage of this is that it provides temperatures over the whole sky. In practice, this instrument also provides information on horizontal spatial characteristics of electron precipitation. An example of the dependence of E_0 on the measured OI (557.7 nm) temperature using the Strickland et al. (1989) model is shown in Fig. 2. The use of this technique will also be described later.

2.2. Instrumentation

Here we briefly describe a typical photometric system developed at The Aerospace Corporation and the technique which these instruments use to determine the three desired parameters, Q, E_0, and f_O.

The photometer has four channels as previously discussed: N_2^+ (427.8 nm; "blue"), OI (630.0 nm; "red"), OI (844.6 nm; "844.6"), and N_2 (871.0 nm). All four filters have bandwidths of between 1 and 2 nm full-width at half-maximum and are typically sampled every 10 s, and the integration time on each filter is typically about 1 s. The photometers look up the local magnetic zenith and the instrument runs automatically from dusk to dawn. A version of this system, at a single site, provided data that were used by Christensen et al. (1997).

All emissions are corrected for backgrounds by subtracting emissions measured during periods of no aurora. Since sometimes auroral emissions continuously occur, fixed backgrounds of less than

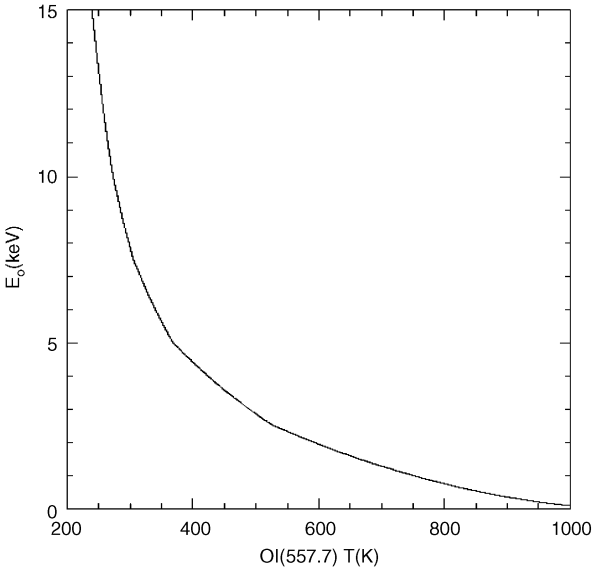

Fig. 2. A plot of the effective temperature of the OI (557.7 nm) as a function of E_0 using the generic GUVI MSIS-90 model atmosphere described in Fig. 1.

100 Ry are subtracted in those cases. These backgrounds are derived from previous measurements. To make sure that background variations do not add significantly to the uncertainty in the derived results, most of the analysis is restricted to periods of bright aurora where the brightness of the blue emission is above 400 Ry. The 871.0/blue ratio is used to correct for atmospheric scattering as described above, and a plot of red/blue versus 8446/blue is used to derive E_0 and f_O. An f_O of 1 indicates no composition change while a factor less than 1 indicates depletion, compared to the model, of atomic oxygen density relative to molecular nitrogen (see below). The blue data can be used to infer Q. It is worth repeating that the 871.0/blue ratio provides a quantitative measure for both correcting for atmospheric scattering and also determining if the sky conditions are adequate for data analysis. For example, as was done in Gattinger et al. (1991), data can be rejected when the ratio becomes too high or too low indicating the presence of very cloudy conditions.

These systems were deployed in Greenland during the 1997–98 winter and in Alaska during January of 1999, and in Alaska from early 2002 to the present. They run continuously and autonomously from dusk to dawn. The data can be retrieved remotely over the internet or via modem. The systems are indoors looking through domes which are warmed by a flow of air and thus kept clear.

Since one use of these data is to compare measured composition changes with auroral energy input, we use a simple standard procedure to approximate the auroral forcing. For particle heating we use the measured Q from our photometer data. For the Joule heating input we use the Delta H component from a magnetometer, the change of the H component from nominally non-auroral conditions, to indicate Joule heating (Duboin and Kamide, 1984). The value of (Delta H)^2 in units of (nT)^2 can be used, when multiplied by a constant, taken as 0.8×10^{-4} mJ/(m^2 s) to estimate the Joule heating rate (Hecht et al., 2000), although this approximation may be inaccurate on occasion due to neutral winds (Thayer, 1998). The total energy input is the sum of these two.

2.3. Uncertainties

There are a number of reasons why the derived results may be uncertain and here they are briefly described.

First, there are uncertainties in the calibration of the photometers. Hecht et al. (1999) discussed these and estimated that Q could be uncertain by as much as 25% because it is derived from measurements that depend on absolute calibration. The other two parameters, f_O and E_0, depend on auroral brightness ratios for which these uncertainties are reduced due to cancellation of terms contributing equally to each channel. Thus, the uncertainties in the brightness ratios typically result in uncertainties on the order of 10%, less than those for an absolute calibration.

Second, are errors in the model. These include many of the assumptions discussed in Hecht et al. (1989, 1991). These include cross-sections and assumptions about the shape of the energy spectrum.

Based on comparisons such as were shown in Hecht et al. (1999), some recent unpublished comparisons between ground- and satellite-derived results, and some of the comparisons presented here, we estimate that the total uncertainty in absolute f_O and E_0 including calibration and model errors is typically less than 30%, and often better than 10%.

Nevertheless calibration errors can occur or develop slowly in automated photometric systems. One such cause might be the slow aging of the filters. Those that cause the brightness ratios to be uncertain, in an absolute sense, by 25% can cause errors in E_0 of up to 50% as will be shown.

However, with the exception of specific uncertainties with respect to the use of the red line, which will be further addressed later, *relative* uncertainties should be on the order of 10% or less in the derived quantities.

Finally, there is the problem associated with choosing a model atmosphere. This is associated with the actual physical meaning of the f_O parameter, discussed in detail in Hecht et al. (1989, 1991). The use of f_O has always been additionally obscured by the fact that its physical interpretation is tied to the model atmosphere used in the analysis. For example, the specific MSIS atmosphere during a large geomagnetic storm, say an A_p of 100, may correctly reflect the real atmosphere and thus, the Strickland technique for analyzing the optical data will result in derived f_O values near 1. However, analyzing the same data with an MSIS atmosphere appropriate to a geomagnetically quiet period, such as the model used in Fig. 1, may result in derived f_O values near 0.4 since the real atmosphere is disturbed compared to the assumed atmosphere. A better way of approaching this is to follow Strickland et al. (1995, 2004) who addressed the problem of determining $[O]/[N_2]$ from satellite ultraviolet dayglow data. Since $[O]/[N_2]$ changed as a function of pressure level they suggested an alternative parameter to f_O. Specifically, they picked an arbitrary reference integrated column N_2 of $10^{17}\,cm^{-2}$. For a given model atmosphere they found the altitude at which that occurred and then integrated the [O]. They then took the ratio of the integrated O to 10^{17}. They designated this O/N_2 ratio as that which occurs when f_O is 1. The O/N_2 then scales linearly with f_O. Therefore, the O/N_2 parameter can be used in place of f_O in the Strickland analysis of auroral emissions. The advantage is that results from different model atmospheres can be compared directly. In the example above an f_O of 1 in the disturbed (A_p of 100) MSIS model may be equivalent to an O/N_2 of 0.5 while for an undisturbed MSIS (A_p of 30) an f_O of 1 is equivalent to an O/N_2 of 1.1. The analysis of the data using the latter MSIS results in derived f_O of 0.4 or derived O/N_2 of 0.44. Thus, it is much easier using O/N_2 to see how the choice of the model atmosphere affects the results. (While the results in this paper are quoted using f_O given that this has been done historically, it is anticipated that future comparisons, especially with GUVI, will use O/N_2 as the composition parameter.) In practice it is found that changes of 15% or so occur in f_O and E_0 if an undisturbed, as opposed to the disturbed MSIS model is used during large geomagnetic storms (D. Strickland, private communication, 2004).

3. Results

We present results from four periods to give examples of what can be obtained from this approach and also to illustrate some of the outstanding questions, which arise from the relationship of composition change to Joule heating. Two of these examples have previously been reported and we summarize those results.

3.1. Poker Flat 1994 (Christensen et al., 1997)

During the second Atmospheric Response in Aurora (ARIA 2) campaign out of Poker Flat, Alaska, the four-channel photometer system obtained the data on February 13, 1994 shown in Fig. 3. The top panel shows an example where f_O first decreased by nearly a factor of two, from its pre-storm value, within about 20 min of a moderate auroral substorm heating event. The f_O value took about 2.5 h to recover to its pre-substorm value. At that point another auroral substorm heating event occurred and f_O decreased again. The data-taking ended before the final amount of decrease could be determined, although the decrease that was measured was about half of that in the first substorm. The bottom figure shows the heating rate (energy flux) from both particles and Joule dissipation. The energy fluence, found by integrating the heating rate over the duration of the substorm, is shown between the brackets. It was $190\,J/m^2$ during the first substorm and $150\,J/m^2$ for the second substorm. In these substorm events the energy fluence due to Joule dissipation was over half the total. Christensen et al. (1997) discussed these data and compared them with the predictions of the Sun et al. (1995) general circulation model. They argued that because of the rapid decrease in f_O and the inability of models to reproduce the magnitude of the effect, the composition changes were due to a yet unknown mechanism. They found that the model underpredicted the composition changes by an order of magnitude.

3.2. Greenland, 1998 (Hecht et al., 2000)

In January 1998 two identical auroral photometers were placed at Kangerlussuaq (67°N geographic

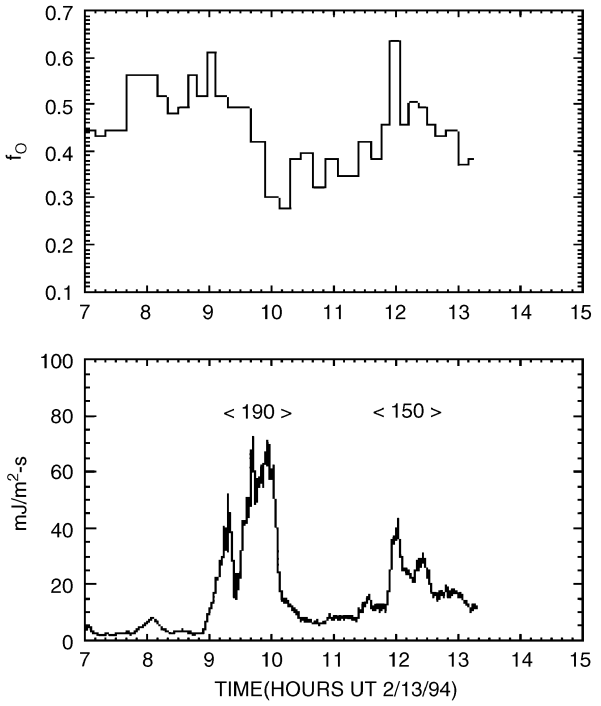

Fig. 3. Top: f_O time series derived from the photometric data obtained on February 13, 1994. Bottom: the corresponding total heating rate that includes both Joule and particle heating. See text for meaning of numbers within bottom panel.

latitude, 74°N geomagnetic latitude) just above the arctic circle in Greenland, and at Narsarsuaq (61°N geographic latitude, 70°N geomagnetic latitude) near the southern tip of Greenland. They are separated by over 700 km. Data were obtained from 2200 UT on January 29, 1998 to 1000 UT on January 30, 1998. The analysis also included data from the Greenland chain of magnetometers, the CANOPUS chain of magnetometers, the Kangerlussuaq radar data, the visible imager on a DMSP satellite, and the PIXIE X-ray instrument (Imhof et al., 1995) on the POLAR satellite. This was the first time that photometric observations of this type were made from two sites simultaneously, and Fig. 4 shows an interesting temporal development of f_O.

At Kangerlussuaq, after 2300 UT, a burst of auroral activity occurred with peak energy deposition rates of 41 mJ/m^2 s. The Joule heating rates of between 5 and 30 mJ/m^2 s, derived from the magnetometer data, compare favorably with those derived from the radar data. The total energy fluence for this event is about 1/4 of that found in Christensen et al. (1997) for the Poker Flat 1994 event which caused a factor of two decrease in f_O. Here the average f_O is about 1.0 with variations of 20% during the event.

During this time period at Narsarsuaq, the energy deposition rates were generally lower, about 10–20 mJ/m^2 s, although because the heating occurred over a longer period the energy fluence was similar to what was found at Kangerlussuaq. However, similar to what was at Poker Flat in 1994, there was a decrease in f_O after the beginning of the event and then a recovery after the event. The average f_O during the event was 0.87.

Around 0030–0100 UT there was a stronger event around Kangerlussuaq with little activity at Narsarsuaq, consistent with the inferences from the radar data that the Joule heating was centered at or to the north of Kangerlussuaq. The Joule heating rates from the magnetometers were again consistent with the radar results. The f_O results resembled those seen at Narsarsuaq during the first event; a decline in f_O at the beginning and a recovery at the end of the event. The average f_O was about 10% lower than was found in the first event.

The third event occurred between 0200 and 0400 UT. The average f_O at Narsarsuaq was 0.78 while at Kangerlussuaq two separate bursts of energetic particles gave average f_O values of 0.96 and 0.88. To summarize, for the period before 0400 UT the average f_O declined about 10% although the auroral energy did cause local changes in f_O of around 30%.

Next we look at the results just from Narsarsuaq after 0400 UT. After about 0430 UT there was almost continuous Joule and particle heating. In the period from 0400 to 0630 UT there was an energy fluence of 96 J/m^2. Before the heating increase began, the f_O values were around 0.7, lower than almost any time prior to this. After the heating increase around 0500 UT, there was a continuous decrease in f_O to values below 0.6. As the heating subsided after 0600 UT the f_O began to increase again. However, around 0700 UT the Joule heating increased and f_O rapidly decreased to values around 0.4. Between 0630 and 0830 the energy fluence was 88 J/m^2 and for the period around 0800 UT the average f_O was around 0.37. Because of the large amounts of auroral energy deposited, these data taken alone seem to be quite consistent with a picture of local depletion of atomic oxygen as discussed above. This is supported by the observations that rapid decreases in f_O are associated with the onset of Joule and/or particle heating events.

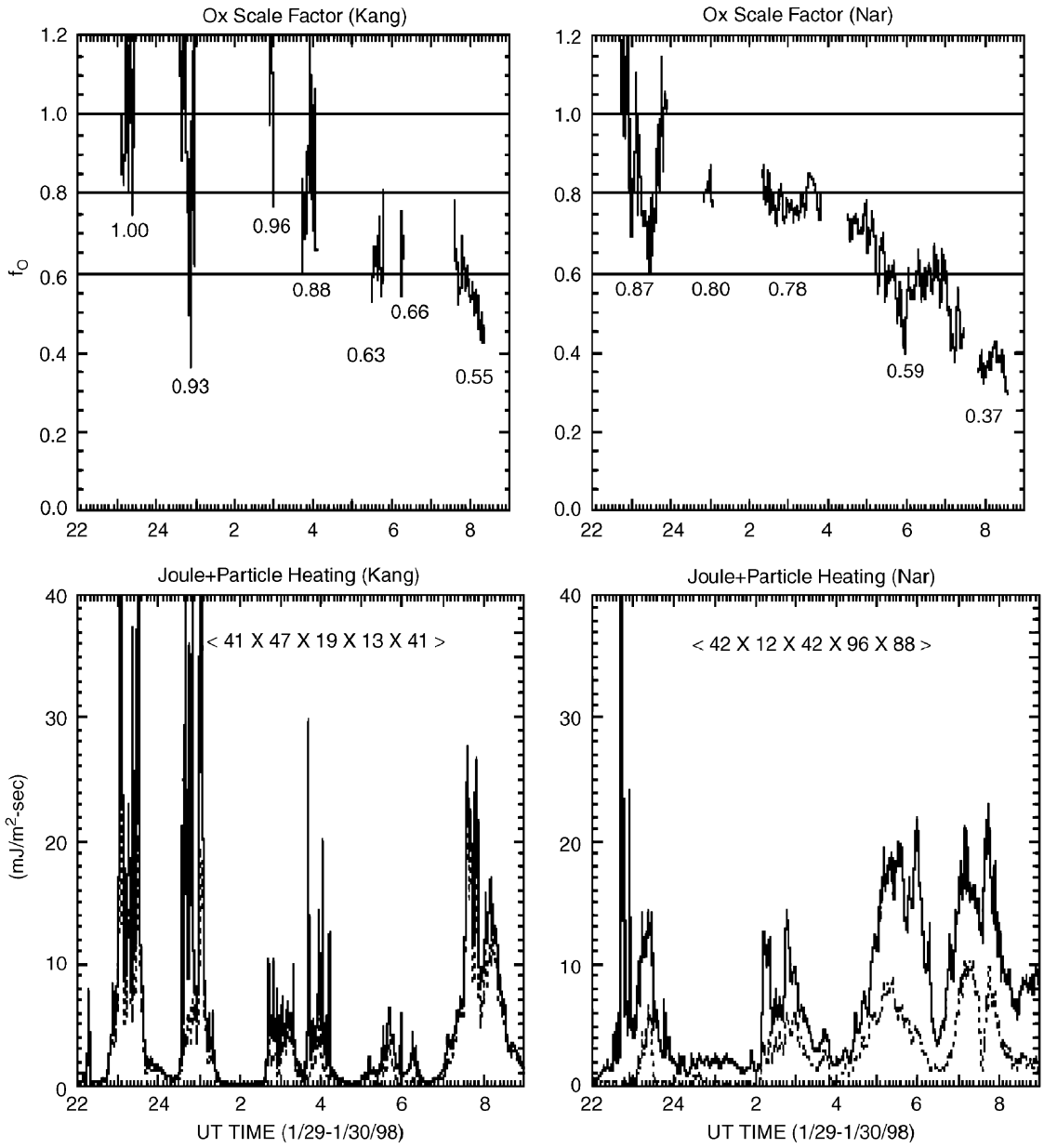

Fig. 4. Time-series plots of the atomic oxygen scaling factor, f_O, and the total heating rate from two sites in Greenland.

However, this picture becomes less clear when simultaneous Kangerlussuaq data are considered. For the period from 0400 to 0700 UT there was almost no energy deposited. Yet the f_O values were about 0.65, almost 1/3 less than was found earlier in the night. After 0730 UT there was a large increase in Joule heating accompanied by a decrease in f_O. While the decrease may have been due to this local heating event, the average value for f_O of about 0.55 is much less than earlier in the night.

While some of these results can partially be explained by the rapid depletions being caused by local heating, such a mechanism cannot explain all the data, especially the Kangerlussuaq data after 0400 UT. An explanation for those results is most probably atomic oxygen depleted air being blown over western Greenland. Auroral activity was centered in Canada, west of Greenland for most of the period from 0400 to 0800 UT. If the winds were blowing towards the east then Greenland

would be receiving O-depleted air. However, given nominal wind velocities of 50 m/s and a time scale of about 2 h between the onset of auroral activity to the west of Kangerlussuaq and the observed decreased f_O around 0600 UT, the depleted air was formed somewhat closer to Kangerlussuaq and thus may still be due to local processes as discussed by Christensen et al. (1997). Nevertheless, these results do show the necessity of considering non-local and local sources in modeling aurorally induced changes in lower thermospheric composition.

3.3. Alaska 1999

These data have not previously been reported in the literature. During the Coupling of Dynamics and Aurora (CODA) rocket experiment, launched from Poker Flat Alaska on January 22 1999, ground-based photometer systems were deployed at two Alaska sites, Poker Flat (65.7N, 147.4W), and Fort Yukon (66.6N, 145.3W) which are separated by a little over 100 km. Data were obtained over six nights and Fig. 5 shows results from Fort Yukon (FY column) and Poker Flat (PK column) on January 14th, a night of high auroral activity. Row (a), at the top, shows the derived f_O values along with a solid curve for an MSIS O/N_2 ratio. The latter ratio is formed by simply dividing [O] and [N_2] at 120 km altitude from the MSIS model for January 14th. The ratio curve is normalized to its value at 120 km on January 8, during a period of low auroral activity at 0900 UT.

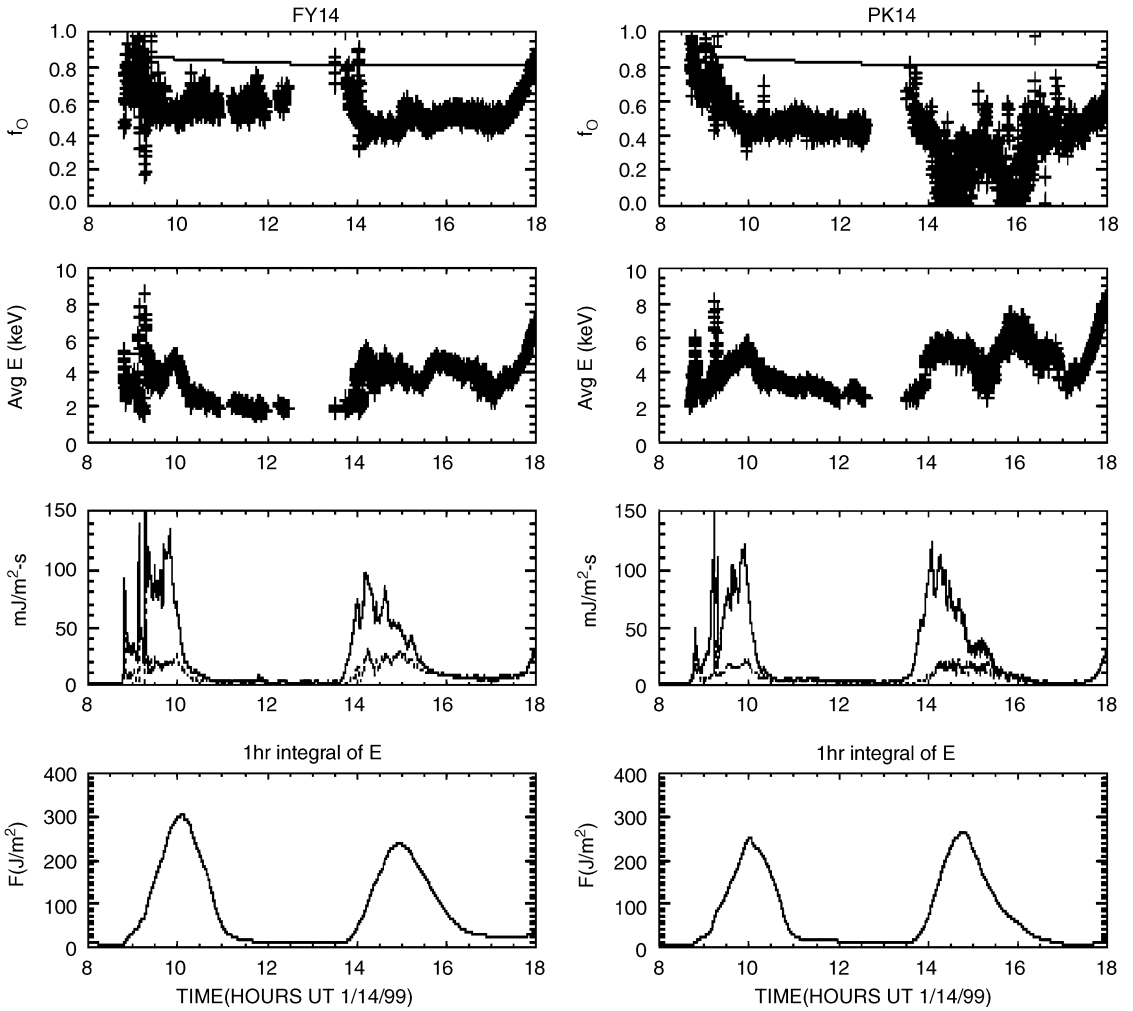

Fig. 5. Plots of f_O, (row a) average energy (row b), heating rate (row c), and energy fluence (row d) derived from data at Fort Yukon (left) and Poker Flat (right) on January 14, 1999.

This curve allows one to see what magnitude depletions MSIS is predicting due to the observed auroral activity. Row (b) shows the average energy, E, which can be derived from E_0. The value of E is twice E_0 if a Maxwellian distribution is used but equal to E_0 if a Gaussian is used. Photometer data were only analyzed when the Blue brightness was greater than 300 Rayleighs (R) (approximately 1.5 mJ/m^2-s). Row (c) shows the heating rate (Joule + particle) in mJ/m^2-s. Row (d) shows the energy fluence, F (J/m^2), for integrated periods of one hour. The results in rows (c) and (d) show the occurrence of two substorms. At the beginning of each substorm the f_O value was approximately represented by the normalized MSIS value. After the substorm began, f_O rapidly decreased and then stayed either constant until the beginning of the next substorm or quite slowly recovered. The responses at the two sites showed some differences and similarities. The differences are especially noticeable during the second substorm where the f_O is much more variable over Poker than at Fort Yukon. Also at the beginning of the second substorm over Poker f_O is quite high compared to its value 2 h earlier. The two hour data gap is large enough so that we cannot be sure whether or not complete recovery occurred. Complicating the interpretation is the apparent inverse relationship in these data at the beginning of the second substorm between the average energy and f_O. This suggests that we may also be sampling composition change at different altitudes.

Fig. 6 shows the average percentage difference between f_O and the normalized MSIS value for each of the six nights and plots it against the energy fluence (J/m^2) for that night. In this plot we also include similar results from our previous data sets collected at Kangerlussuaq in 1987 and 1998, Narsarsuaq in 1998, and Poker in 1994. (For Poker 1994 data, we used the quiet time f_O value in place of the normalized MSIS value). Also shown are two fits, one linear and one a second-order polynomial. In Fig. 7 we plot the % change in f_O, from either the MSIS value or in the case of the Poker 1994 data from the f_O value at the beginning of the substorm versus energy fluence over the substorm. In both cases we see a general trend of decreasing f_O as the energy fluence increases. Again two model fits are shown. However, the exact shape of the relationship

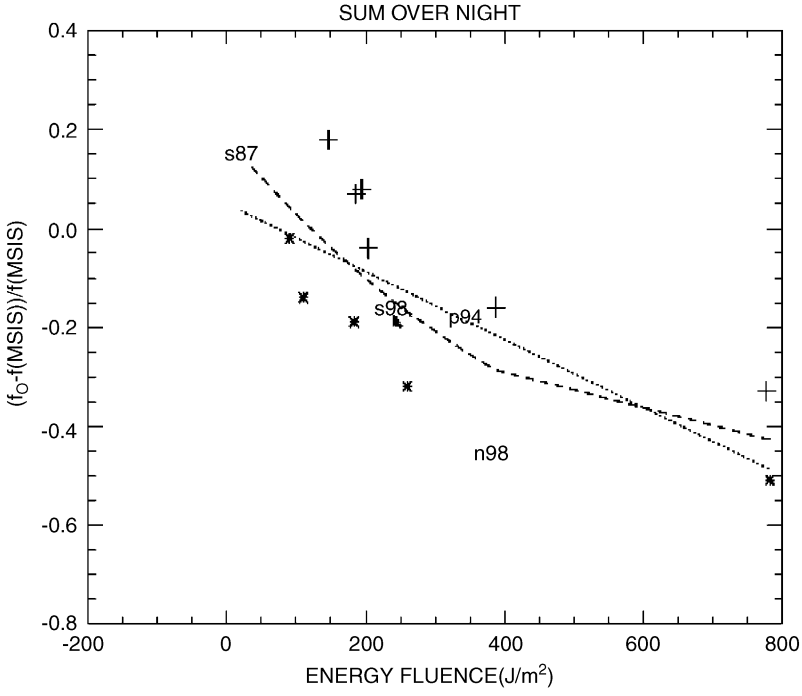

Fig. 6. The average percentage difference between f_O and MSIS for each night plotted vs. energy fluence. Symbols are as follows: + represents Fort Yukon data from 1/99, * represents Poker Flat data for 1/99, s87 are data from Kangerlussuaq in 1987 (Niciejewski et al., 1989), s98 and n98 are from Greenland in 1998 (Hecht et al., 2000), and p94 is from Poker Flat Alaska in 1994. A linear (dotted line) and a second-order polynomial fit (dashed line) are shown.

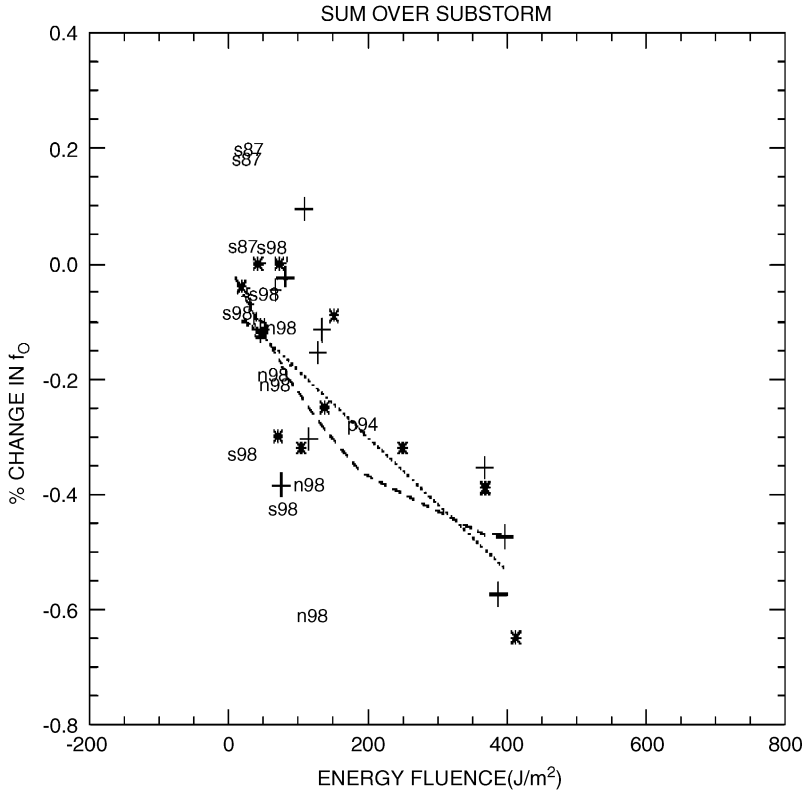

Fig. 7. Same symbols as in Fig. 6. Percentage change in f_O from beginning of substorm vs. energy fluence.

(linear or quadratic) needs further data as they both yield the same experimental variance (Bevington, 1969). Thus, there are two outstanding questions that arise from these observations which have still not been fully resolved. (1) What is the relative importance of local mechanisms versus transport in the composition changes we observe? (2) What is the form of the relationship between energy input and observed composition change?

3.4. Alaska—Poker Flat/Fort Yukon 2002–04

The GUVI instrument on TIMED uses a variation of the photometric technique described above to be able to retrieve E_0 and f_O. E_0 is obtained by the ratio of two different N_2 LBH emissions (LBH long and short) which are absorbed differently by molecular oxygen. The value for f_O is obtained by taking the ratio of OI (135.6 nm) to LBH long. Since all the emissions originated mainly in the lower E region (like blue and 844.6) the GUVI data provide a means of retrieving composition changes in the 100–200 km region without the problems associated with the red line. Although low altitude satellite observations over a given auroral location occur approximately every 100 min, and revisit time may only occur on a few orbits a day, GUVI can also obtain f_O from dayglow emissions. Thus, GUVI observations can provide a global picture of composition change over a restricted local time. This complements very well ground-based observations using the photometric technique which can provide data on f_O at a single location but as a function of time thus capturing the short time scale dynamic effects not accessible to GUVI.

As part of the GUVI validation effort the two photometers described above were placed at Fort Yukon and Poker Flat where they have been operating since early 2002 during the auroral season (generally October to early May). The objective was to compare the ground-based results with the satellite results during favorable overpasses and also to see how the local composition changes compared to the global response during active geomagnetic storm periods. The location at Poker Flat also allows the OI (557.7 nm) temperature data, obtained from the Conde/Smith Scanning Doppler Interferometer, to be used to derive E_0. Thus, one

can compare f_O derived using two independent ground-based techniques; (a) E_0 and f_O derived from red/blue vs. 844.6/blue, (b) E_0 derived from the OI (557.7 nm) temperature and f_O derived from this E_0 and 844.6/blue.

In addition, we evaluate the dependence of the OI (557.7 nm)/blue ratio as a possible measure of f_O. A model plot of this OI (557.7 nm)/blue vs. red/blue is shown in Fig. 8. As can be seen, the OI (557.7 nm)/blue ratio is not very sensitive to E_0 but is strongly dependent on f_O. Based on the Strickland et al. (1989) model results, this is due to the primary excitation being an energy transfer from excited $N_2(A)$ to atomic oxygen atoms that causes OI (557.7 nm) emission. Measurements of this ratio will follow in addition to those for red/blue and 844.6/blue.

The Scanning Doppler Interferometer data allow a measure of the OI (555.7 nm) brightness. However, these brightness data are not well calibrated, in an absolute sense. Since we are interested in relative changes an arbitrary calibration can be applied in order to simply show the relative variations over the night. However, the Poker Flat Observatory also includes a Meridian Scanning Photometer (MSP) that measures both OI (557.7 nm) and blue. Thus, all of the OI (555.7 nm)/blue ratios are taken from the MSP scans looking up the magnetic zenith. A comparison was also made between the relative variations of the MSP and Conde/Smith OI (555.7 nm) data and they did not appreciably differ. Thus, we have another measure of f_O independent of OI (844.6 nm) data.

The comparisons shown next are from data collected on November 16, 2003 at Poker Flat. Fig. 9 shows the blue emission during periods where it exceeded approximately $1000R$ which corresponds to a Q value of $\sim 4\,\mathrm{mJ/m^2\,s}$. These brightnesses are large enough so that any uncertainty in background correction would be negligible.

Fig. 10 shows comparisons between red/blue and 844.6/blue (top), red/blue and OI (557.7 nm)/blue (middle) and the variation of red/blue vs. the OI (557.7 nm) temperature variation (bottom). Recall

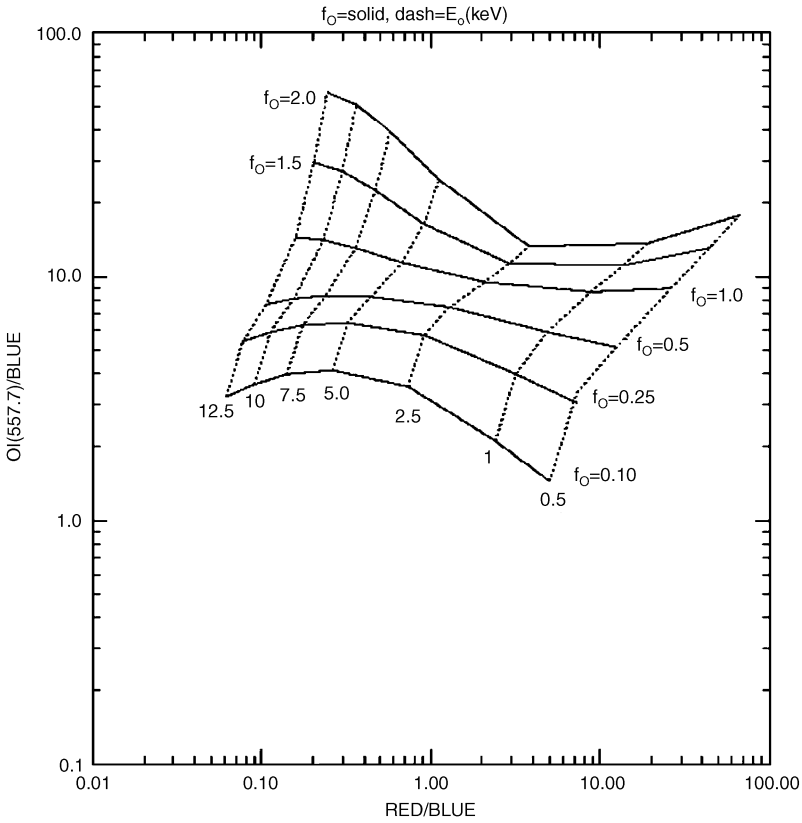

Fig. 8. A plot of red/blue vs OI (557.7 nm)/blue as a function of E_0 and f_O. Gaussian distributions with high and low energy tails are used to characterize electron precipitation.

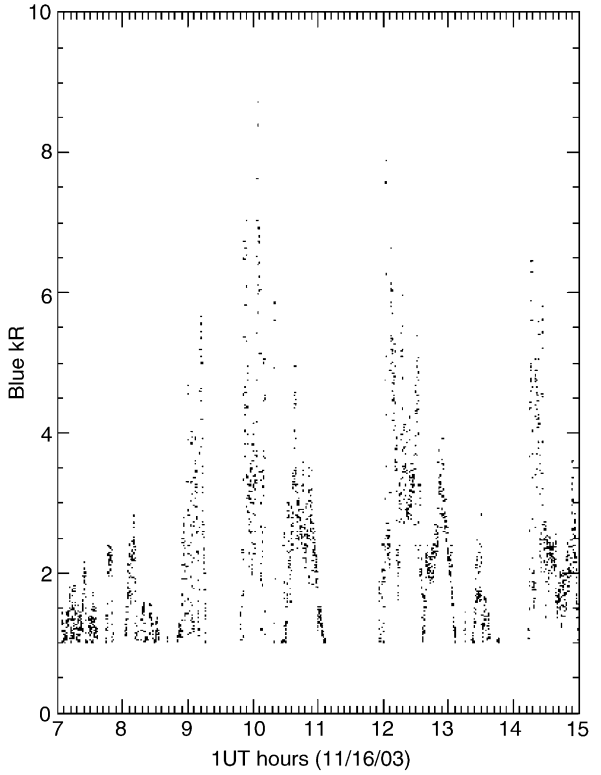

Fig. 9. A plot of blue emission in kR vs time on November 16, 2003 during periods where it exceeded 1 kR.

that as a function of E_0, red/blue has the greatest variation and OI (557.7 nm)/blue has the least while the reverse is true as a function of f_O. The middle panel shows that the OI (557.7 nm)/blue ratios are relatively flat suggesting relatively little variation in f_O. The bottom panel shows significant variations in red/blue and OI (557.7 nm) temperature suggesting a considerable variation in E_0. Here it is shown that for the most part, red/blue varies with temperature as expected; an increase in red/blue corresponds to higher OI (557.7 nm) temperatures coincident with lower energy particle precipitation. Thus, we expect that some but not all of the variations in 844.6/blue are due to that ratios dependence on E_0. The variation of 844.6/blue as a function of E_0 is probably best seen between the regions around 8 and 10 UT where 844.6/blue is varying while OI (557.7 nm)/blue is nearly constant and in the period from 1430 to 1500 UT.

The derivations of E_0 and f_O using the two techniques discussed above are shown in Fig. 11. The E_0s derived from the OI (557.7 nm) temperatures are higher than when red/blue is used but are fairly consistent. The f_O values derived from the OI (557.7 nm) temperatures are somewhat lower although vary in a similar manner similar except perhaps between 7 and 8 UT where they appear to be relatively lower. The E_0 values are from 0 to 50% higher when the temperature technique is used in place of red/blue. In most cases however, there were only modest changes in f_O during the night, consistent with a relatively low energy fluence of less than 10 J/m^2, as derived from the particle data above, and from Poker Flat magnetometer data.

Differences between the two may be partly due to calibration. It was found (not shown) that errors of 10% in calibration of the absolute red/blue ratio translated into an equivalent uncertainty in the two derived quantities, E_0 and f_O. Another possibility is an incorrect temperature profile perhaps due to wave activity not captured in the MSIS atmosphere (see below).

The one period where calibration issues cannot explain the differences is between 7 and 8 UT. Even with the calibration adjustment the energies derived using red to blue are lower. This is probably real because the red emission is quite sensitive to low energy electrons compared to the other OI emissions.

The influence of low energy electrons is to be explored in a future publication, and its occurrance suggests some caution needs to be used in interpreting the results of these ground-based measurements. The following points expand upon this and add further discussion about potential improvements to our remote sensing technique with the addition of the OI (557.7 nm) feature:

1. During a large magnetic storm, variations in the occurrence of intense low energy precipitation or possible deviations from MSIS in the shape of the O density profile between the E and F regions can distort the analysis of red/blue and 844.6/blue. In particular it was found on November 20, 2003, when K_p reached 9-, that E_0 values inferred from the photometric data were sometimes a factor of two lower than those inferred from the OI (557.7 nm) temperatures. During TIMED overpasses, GUVI-derived E_0 values were observed to be in agreement with those from the OI (557.7 nm) temperature measurements (D. Strickland, private communication, 2004). When those E_0 values were used in conjunction with 844.6/blue, the ground-based and GUVI, f_O values were in reasonable agreement. Thus, inference of O densities in the E region may be somewhat

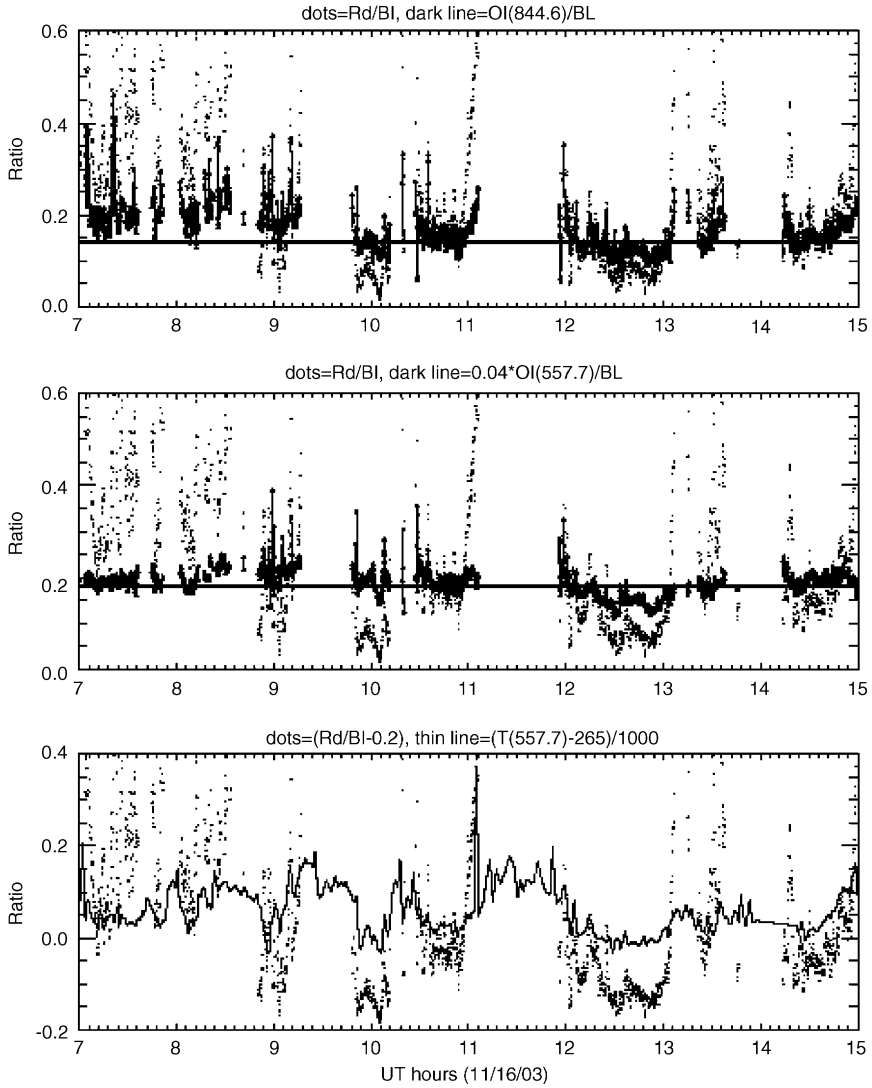

Fig. 10. Three panels show comparisons between (top) red/blue and 844.6/blue, (middle) red/blue and OI (557.7 nm)/blue plus 0.05, and (bottom) the variation of red/blue vs. the OI (557.7 nm) temperature variation. The horizontal lines are shown to guide the eye as the ratios vary throughout the night. Dots are used for red/blue in all three panels.

distorted during large geomagnetic superstorms if red line emission is solely used in the analysis. Thus, the analysis of f_O variations during the large geomagnetic storm in February 1986 by Hecht et al. (1991) did not principally rely on red line data because of concerns like those just expressed. We note, however, that comparisons outside this storm period show generally good agreement between the photometric red/blue vs. 844.6/blue technique and GUVI data although some calibration adjustment (on the order of 25%) may have to be applied to the ground-based data.

2. Fig. 2 shows that the OI (557.7 nm) temperature technique becomes somewhat insensitive at high E_0s. Thus, small temperature changes in the actual atmospheric temperature profile, caused by gravity waves or tidal activity, and which are not captured in a model atmosphere, can result in an error in derived E_0. This is especially true for energetic electrons that may be deposited near 100 km, a region of known variable wave activity. The sensitivity of this technique is height dependent so that temperature variations by waves do not cause much E_0 variation at high altitudes.

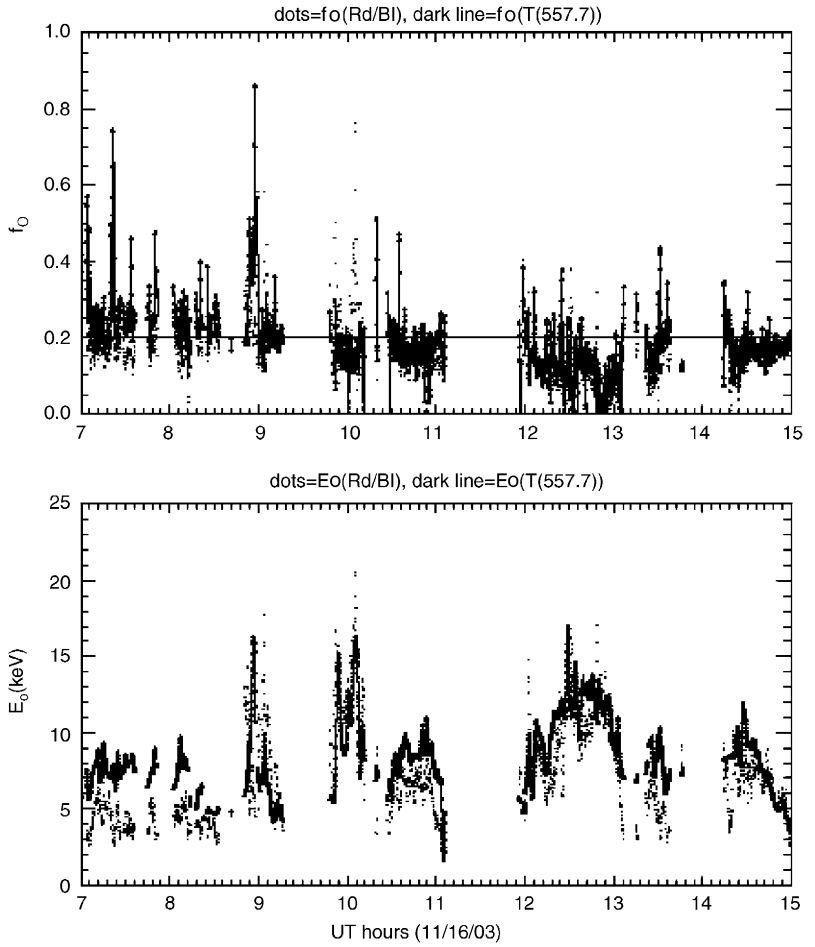

Fig. 11. The two panels show E_0 and f_O derived from two techniques. They are (1) red/blue vs. 844.6/blue used to derive E_0 and f_O, or (2) E_0 from OI (557.7 nm) temperatures and f_O derived from a combination of that E_0 and 844.6/blue. Dots are used for the first technique and a solid line connecting triangles is used for the second technique: (top) derived f_O vs time on November 16, 2003, (bottom) derived E_0 vs. time. Both derivations apply only to periods when the blue emission exceeded 1 kR.

3. Furthermore, red/blue vs. OI (555.7 nm)/blue may also be a candidate for determining E_0 and f_O. This could open up a wealth of meridian scanning photometer data that could be analyzed for f_O variations.

4. Conclusions

The use of passive ground-based optical remote sensing to monitor auroral energy deposition has been shown to be a viable technique. Relatively inexpensive photometers can be used to monitor the energy flux of precipitating particles, and, with a judicious choice of filters, both the characteristic energy of precipitating particles, and changes in composition (reflected through either f_O or the O/N_2 column density ratio). As noted above, some caution needs to be used in applying this technique. But given that several independent measurements can be made of the same quantity, we would recommend that future ground-based observatories be equipped with filter photometers that can measure the following emissions discussed above: OI (630.0 nm), OI (844.6 nm), OI (557.7 nm), N_2^+ (427.8 nm), and N_2 (871.0 nm). This should be supplemented by measurements of the OI (557.7 nm) and OI (630.0 nm) temperatures using the Conde/Smith technique. These measurements would allow a further independent check on E_0 via OI (557.7 nm) data, and the exospheric temperature, which is needed to validate the model atmosphere

temperature predictions, via OI (630.0 nm). These data taken together would allow a reliable measurement of f_O and E_0 as each is measured independently more than once. All but the OI (630.0 nm) temperature data are available for the past few years at the Poker Flat Observatory.

In the future one would expect in principle that information could be obtained not only on E region composition changes using OI (557.7 nm) temperature and brightness data along with N_2^+ (427.8 nm,) but perhaps also in the F region using OI (844.6 nm) and OI (630.0 nm) data. However, in the immediate future enough data should exist to answer one of the questions posed earlier, namely how does the change in the O/N_2 ratio in the thermosphere scale with auroral activity.

Acknowledgments

Support was provided by NASA Grant no. NAG5-10252 and by The Aerospace Corporation's Mission Oriented Investigation and Experimentation program, funded by the US Air Force Space and Missile Systems Center under Contract no. FA8802-04-C-0001.

References

Anderson, P.C., et al., 1995. The ARIA I rocket campaign. Journal of Geophysical Research 100, 17,265–17,284.

Bevington, P.R., 1969. Data Reduction and Error Analysis for the Physical Sciences. McGraw-Hill Book Company, New York, NY.

Burns, A.G., Killeen, T.L., Roble, R.G., 1991. A theoretical study of thermospheric composition perturbations during an impulsive geomagnetic storm. Journal of Geophysical Research 96, 14,153–14,167.

Burns, A.G., Killeen, T.L., Deng, W., Carignan, G.R., 1995. Geomagnetic storm effects in the low- to middle-latitude upper thermosphere. Journal of Geophysical Research 100, 14,673–14,692.

Christensen, A.B., Hecht, J.H., Walterscheid, R.L., Larsen, M.F., Sharp, W.E., 1997. Depletion of oxygen in aurora: evidence for a local mechanism. Journal of Geophysical Research 102, 22,273–22,277.

Christensen, A.B., et al., 2003. Initial observations with the Global Ultraviolet Imager (GUVI) in the NASA TIMED satellite mission. Journal of Geophysical Research 108 (A12), 1451.

Conde, M., Smith, R.W., 1998. Spatial structure in the thermospheric horizontal wind above Poker Flat, Alaska, during solar minimum. Journal of Geophysical Research 103, 9449–9472.

Craven, J.D., Nicholas, A.C., Frank, L.A., Strickland, D.J., 1994. Variations in FUV dayglow brightness following intense auroral activity. Geophysical Research Letters 21, 2793–2796.

Drob, D.P., Meier, R.R., Picone, J.M., Strickland, D.J., Cox, R.J., Nicholas, A.C., 1999. Atomic oxygen in the thermosphere during the July 13, 1982 solar proton event deduced from far ultraviolet images. Journal of Geophysical Research 104, 4267–4278.

Duboin, M., Kamide, Y., 1984. Latitudinal variations of Joule heating due to the auroral electrojets. Journal of Geophysical Research 89, 245–251.

Fuller-Rowell, T.J., 1985. A two-dimensional high-resolution nested-grid model of the thermosphere. 2. Response of the thermosphere to narrow and broad electrodynamic features. Journal of Geophysical Research 90, 6567–6586.

Fuller-Rowell, T.J., Codrescu, M.V., Moffett, R.J., Qeugan, S., 1994. Response of the thermosphere and ionosphere to geomagnetic storms. Journal of Geophysical Research 99, 3893–3914.

Fuller-Rowell, T.J., Codrescu, M.V., Rishbeth, H., Moffett, R.J., Qeugan, S., 1996. On the seasonal response of the thermosphere and ionosphere to geomagnetic storms. Journal of Geophysical Research 101, 2343–2354.

Gattinger, R.L., Jones, A.V., Hecht, J.H., Strickland, D.J., Kelly, J., 1991. Comparison of ground-based optical observations of N_2 second positive to N_2^+ first negative emission ratios with electron precipitation energies inferred from the Sondre Stromfjord radar. Journal of Geophysical Research 96, 11,341–11,352.

Hays, P.B., Jones, R.A., Rees, M.H., 1973. Auroral heating and the composition of the neutral atmosphere. Planetary and Space Science 21, 559–573.

Hecht, J.H., Christensen, A.B., Pranke, J.B., 1985. High-resolution auroral observations of the OI (7774) and OI (8446) multiplets. Geophysical Research Letters 12, 605–608.

Hecht, J.H., Christensen, A.B., Strickland, D.J., Meier, R.R., 1989. Deducing composition and incident electron spectra from ground-based auroral optical measurements: variations in oxygen density. Journal of Geophysical Research 94, 13,553–13,563.

Hecht, J.H., Strickland, D.J., Christensen, A.B., Kayser, D.C., Walterscheid, R.L., 1991. Lower thermospheric composition changes derived from optical and radar data taken at Sondre Stromfjord during the great magnetic storm of February, 1986. Journal of Geophysical Research 96, 5757–5776.

Hecht, J.H., Christensen, A.B., Gutierrez, D.J., Sharp, W.E., Sharber, J.R., Winningham, J.D., Frahm, R.A., Strickland, D.J., McEwen, D.J., 1995. Observations of the neutral atmosphere between 100 to 200 km using ARIA rocketborne and ground-based instruments. Journal of Geophysical Research 100, 17,285–17,298.

Hecht, J.H., Christensen, A.B., Strickland, D.J., Majeed, T., Gattinger, R.L., Vallance Jones, A., 1999. Comparison between auroral particle characteristics and atmospheric composition inferred from analyzing optical emission measurements alone and in combination with incoherent scatter radar measurements. Journal of Geophysical Research 104, 33–44.

Hecht, J.H., McKenzie, D.L., Christensen, A.B., Strickland, D.J., Thayer, J.P., Watermann, J., 2000. Simultaneous observations of lower thermospheric composition change during moderate auroral activity from Kangerlussuaq and

Narsarsuaq, Greenland. Journal of Geophysical Research 105, 27,109–27,118.

Hedin, A.E., 1983. A revised thermospheric model based on mass spectrometer and incoherent scatter radar data: MSIS-83. Journal of Geophysical Research 88, 10,170–10,188.

Immel, T.J., Craven, J.D., Frank, L.A., 1997. Influence of IMF B_y on large-scale decreases of O column density at middle latitudes. Journal of Atmospheric and Solar-Terrestrial Physics 59, 725.

Imhof, W.L., et al., 1995. The Polar Ionospheric X-ray Imager Experiment (PIXIE). In: Russell, C.T. (Ed.), The Global Geospace Mission. Kluwer Academic Publishers, Dordrecht, pp. 385–408.

Mayr, H.G., Volland, H., 1973. Magnetic storm characteristics of the thermosphere. Journal of Geophysical Research 78, 2251–2264.

Meier, R.R., Strickland, D.J., Hecht, J.H., Christensen, A.B., 1989. Deducing composition and incident electron spectra from ground-based auroral optical measurements: a study of auroral red line processes. Journal of Geophysical Research 94, 13,541–13,552.

Niciejewski Jr., R.J., McCormac, F.G., Hecht, J.H., Christensen, A.B., Sivjee, G.G., Strickland, D.J., Swenson, G., Mende, S.B., Jones, A.V., Gattinger, R.L., Carlson, H.C., Valladares, C.E., 1989. Coordinated satellite and ground-based measurements of the energy characteristics of a sun-aligned arc over Søndre Strømfjord. Journal of Geophysical Research 94, 17,201–17,213.

Nicholas, A.C., Craven, J.D., Frank, L.A., 1997. A survey of large-scale variations in thermospheric oxygen column density with magnetic activity as inferred from observations of the FUV dayglow. Journal of Geophysical Research 102, 4493–4510.

Rees, M.H., Luckey, D., 1974. Auroral electron energy derived from ratio of spectroscopic emissions 1. Model computations. Journal of Geophysical Research 79, 5181–5186.

Sivjee, G.G., Shen, D., 1997. Auroral optical emissions during the solar magnetic cloud event of October 1995. Journal of Geophysical Research 102, 7431–7438.

Sivjee, G.G., Shen, D., Yee, J.H., Romick, G.J., 1999. Variations, with peak emission altitude, in auroral O_2 atmospheric (1, 1)/(0, 1) ratio and its relation to other auroral emissions. Journal of Geophysical Research 104, 28,003–28,018.

Strickland, D.J., Meier, R.R., Hecht, J.H., Christensen, A.B., 1989. Deducing composition and incident electron spectra from ground-based auroral optical measurements: theory and model results. Journal of Geophysical Research 94, 13,527–13,539.

Strickland, D.J., Daniell Jr., R.E., Jasperse, J.R., Basu, B., 1993. Transport-theoretic model for the electron–proton–hydrogen atom aurora: 2. Model results. Journal of Geophysical Research 98, 21,533–21,548.

Strickland, D.J., Evans, J.S., Paxton, L.J., 1995. Satellite remote sensing of thermospheric O/N_2 and solar EUV: 1. Theory. Journal of Geophysical Research 100, 12,217–12,226.

Strickland, D.J., Cox, R.J., Meier, R.R., Drob, D.P., 1999. Global O/N_2 derived from DE-1 FUV imaging dayglow data: technique and examples from two storm periods. Journal of Geophysical Research 104, 4251–4266.

Strickland, D.J., Hecht, J.H., Christensen, A.B., McEwen, D.J., 2000. Thermospheric disturbance recorded by photometers on-board the ARIA II rocket. Journal of Geophysical Research 105, 2461–2476.

Strickland, D.J., Meier, R.R., Walterscheid, R.L., Craven, J.D., Christensen, A.B., Paxton, L.J., Morrison, D., Crowley, G., 2004. Quiet-time seasonal behavior of the thermosphere seen in the far ultraviolet dayglow. Journal of Geophysical Research 109, A01302.

Sun, Z.-P., Turco, R.P., Walterscheid, R.L., Venkateswaren, S.V., Jones, P.W., 1995. Thermospheric response to morning-side diffuse aurora: high-resolution three dimensional simulations. Journal of Geophysical Research 100, 23,779–23,793.

Thayer, J.P., 1998. Height-resolved Joule heating rates in the high-latitude E region and the influence of neutral winds. Journal of Geophysical Research 103, 471–487.

Vallance Jones, A., 1974. Aurora. D. Reidel, Norwood MA.

Vallance Jones, A., Gattinger, R.L., Shih, P., Meriwether, J.W., Wickwar, V.B., Kelly, J., 1987. Optical and radar characterization of a short-lived auroral event at high latitude. Journal of Geophysical Research 92, 4575–4589.